The Coordination of Leaf Photosynthesis Links C and N Fluxes in C_3 Plant Species

Vincent Maire[1]*, Pierre Martre[2,3], Jens Kattge[4], François Gastal[5], Gerd Esser[6], Sébastien Fontaine[1], Jean-François Soussana[1]*

1 INRA, UR874 UREP, Clermont-Ferrand, France, 2 INRA, UMR1095 GDEC, Clermont-Ferrand, France, 3 Blaise Pascal University, UMR1095 GDEC, Aubière, France, 4 Max Planck Institute for Biogeochemistry, Jena, Germany, 5 INRA, UR4 P3F, Lusignan, France, 6 Justus Liebig University, Institute for Plant Ecology, Giessen, Germany

Abstract

Photosynthetic capacity is one of the most sensitive parameters in vegetation models and its relationship to leaf nitrogen content links the carbon and nitrogen cycles. Process understanding for reliably predicting photosynthetic capacity is still missing. To advance this understanding we have tested across C_3 plant species the coordination hypothesis, which assumes nitrogen allocation to photosynthetic processes such that photosynthesis tends to be co-limited by ribulose-1,5-bisphosphate (RuBP) carboxylation and regeneration. The coordination hypothesis yields an analytical solution to predict photosynthetic capacity and calculate area-based leaf nitrogen content (N_a). The resulting model linking leaf photosynthesis, stomata conductance and nitrogen investment provides testable hypotheses about the physiological regulation of these processes. Based on a dataset of 293 observations for 31 species grown under a range of environmental conditions, we confirm the coordination hypothesis: under mean environmental conditions experienced by leaves during the preceding month, RuBP carboxylation equals RuBP regeneration. We identify three key parameters for photosynthetic coordination: specific leaf area and two photosynthetic traits (k_3, which modulates N investment and is the ratio of RuBP carboxylation/oxygenation capacity ($V_{C_{max}}$) to leaf photosynthetic N content (N_{pa}); and J_{fac}, which modulates photosynthesis for a given k_3 and is the ratio of RuBP regeneration capacity (J_{max}) to $V_{C_{max}}$). With species-specific parameter values of *SLA*, k_3 and J_{fac}, our leaf photosynthesis coordination model accounts for 93% of the total variance in N_a across species and environmental conditions. A calibration by plant functional type of k_3 and J_{fac} still leads to accurate model prediction of N_a, while *SLA* calibration is essentially required at species level. Observed variations in k_3 and J_{fac} are partly explained by environmental and phylogenetic constraints, while *SLA* variation is partly explained by phylogeny. These results open a new avenue for predicting photosynthetic capacity and leaf nitrogen content in vegetation models.

Citation: Maire V, Martre P, Kattge J, Gastal F, Esser G, et al. (2012) The Coordination of Leaf Photosynthesis Links C and N Fluxes in C_3 Plant Species. PLoS ONE 7(6): e38345. doi:10.1371/journal.pone.0038345

Editor: Ben Bond-Lamberty, DOE Pacific Northwest National Laboratory, United States of America

Received December 27, 2011; **Accepted** May 3, 2012; **Published** June 7, 2012

Funding: This study contributes to the French ANR DISCOVER project (ANR-05-BDIV-010-01). VM was funded by a PhD grant of the French research ministry (MENRT). The funders had no role in study design, data collection and analysis, decision to publish, or preparation of the manuscript.

Competing Interests: The authors have declared that no competing interests exist.

* E-mail: jfsoussana@clermont.inra.fr (JFS); vmaire24@gmail.com (VM)

Introduction

The response of leaf net photosynthesis to variations in light, temperature and CO_2 concentration has been successfully represented by the biochemical model of C_3 photosynthesis proposed by Farquhar, von Caemmerer and Berry [1]. This model has pioneered the mechanistic representation of the main biochemical processes of leaf photosynthesis, based on the assumption that photosynthesis is limited by either the carboxylation/oxygenation of ribulose-1,5-bisphosphate (RuBP) by the enzyme ribulose 1·5-bisphosphate carboxylase/oxygenase (Rubisco; W_c), or the regeneration of RuBP by the electron transport chain (W_j). Maximum rates of these two processes are determined by carboxylation capacity ($V_{C_{max}}$) and electron transport capacity (J_{max}). A strong correlation linearly links the variations of $V_{C_{max}}$ and J_{max} across species (*e.g.* [2]) and environmental conditions during plant growth (*e.g.* [3,4]). Since both capacities are measured independently, this result suggests that CO_2 assimilation is regulated in a coordinated manner by these two processes [5].

The variations of net photosynthesis with growth condition, season and species, are related to concurrent changes in leaf nitrogen content (N_a) and to the allocation of nitrogen between different protein pools [6]. $V_{C_{max}}$ and J_{max} linearly correlate with N_a at both intra-and-interspecific levels [3,4,7]. Nevertheless, so far the relationship between $V_{C_{max}}$ and J_{max} and their link to N_a are empirical correlations, their scatter is substantial, and a predictive process understanding C–N coupling at the leaf scale is still missing. As photosynthetic capacity is among the most influential parameters in current vegetation models [8], such an understanding is essential to predict photosynthesis at leaf, plant, stand and ecosystem scales under changing environmental conditions.

Haxeltine and Prentice [9] suggested a general model for the light-use efficiency of primary production, which links photosynthetic capacity and N_a. This model is based on the Farquhar's model of photosynthesis and has been implemented in the global terrestrial vegetation model LPJ [10]. This approach does not account for N limitation and is based on the optimization theory that maximizes assimilation against incoming radiation. Until now, a clear understanding of leaf N variations along vegetative canopies as well as across species and environments has not been provided by the optimization theory [11,12]. For instance, all reported studies observed N gradients less steep than predicted with the optimization theory, suggesting that it likely overestimates predicted C gain [13–18]. Moreover, there are several limitations in optimization theory calculations (for a detailed discussion, see [19]).

Chen et al. [20] proposed an alternative approach: the coordination hypothesis of leaf photosynthesis. The basic assumption of this approach is that $V_{C_{max}}$ and J_{max} are actively regulated by plants in response to environmental conditions such that for most representative conditions W_c equals W_j. The optimality criterion in this context is not maximum C gain (as proposed in [21–23]), but the balance of RuBP carboxylation and regeneration, providing a coordinated allocation of resources, *i.e.* nitrogen, to these two photosynthetic processes (Fig. S1). For vertical gradients within canopies the co-limiting N content was shown to increase with irradiance and to decline with temperature and with atmospheric CO_2 concentration [20]. In agreement with experimental studies, the coordination hypothesis showed that N distribution with canopy depth declines less than the light gradient [13–18].

However, so far this co-limitation and its link to N_a has been considered only for vertical gradients within plant canopies, and has not yet been studied and validated across plant species and environmental conditions. This is possibly due to a lack of appropriate data including environmental growth conditions and photosynthetic parameters for a range of C_3 plant species. In addition, a full test of this hypothesis requires extending the calculation of the co-limiting N content to account for the coupling between leaf photosynthesis and stomatal conductance [3] as well as ascribing leaf N to structural and metabolic pools [24,25].

In this study, we evaluate for the first time the coordination hypothesis for sunlit leaves and its link to N_a for a large range of plant species grown under different environmental conditions. We use an extended version of the Farquhar model of C_3 photosynthesis, a stomatal conductance model and a leaf N model to couple C, N and water fluxes at the leaf scale (see equations and variables in Tables 1–2). We apply this model to a dataset that includes leaf and environmental characteristics during plant growth and gas exchange measurements for a total of 31 C_3 species (293 observations, Table S1). For each observation, plant characteristics included the specific leaf area (SLA, $m^2\ g^{-1}$ DM), N_a ($gN\ m^{-2}$), and $V_{C_{max}}$ and J_{max} ($\mu mol\ m^{-2}\ s^{-1}$) at reference temperature and atmospheric CO_2 concentration. The dataset covers six plant functional types (PFTs) grown both under constant and outdoors environments at a range of N and water supplies and atmospheric CO_2 concentrations.

In agreement with the half-life time of Rubisco [26], we assumed that photosynthetic coordination varies with the mean over one month of the environmental conditions during plant growth. We tested the coordination hypothesis: i) by comparing simulated W_c and W_j values for the measured N_a, and ii) by comparing simulated (N_{ac}) and measured (N_a) leaf N contents. Second, thanks to a statistical model, we distinguished the plant species and environmental conditions effects on leaf photosynthetic traits. Third, we tested the implications of our leaf photosynthesis coordination model for net C assimilation (A_n) and for photosynthetic N use efficiency ($PNUE$) by varying plant photosynthetic traits and environmental growth conditions. Based on these results, we discuss the applicability of the coordination hypothesis to predict photosynthetic capacity and N content of sunlit leaves at the ecosystem and global scales.

Methods

A Model Coupling Leaf N with CO_2 and H_2O Fluxes

Several formulations and parameterizations of the original model by Farquhar et al. [1] have been described. Here, we refer to the formulation and parameterization used by Wohlfahrt et al. [3]. The net rate of C assimilation (A_n, $\mu mol\ m^{-2}\ s^{-1}$) was limited either by carboxylase activity of Rubisco (W_c, $\mu molCO_2\ m^{-2}\ s^{-1}$) or by electron flux through the chloroplast photosystems (W_j, $\mu molCO_2\ m^{-2}\ s^{-1}$) (see Eqn 3–4, 7 in Table 1). Their respective capacity, $V_{C_{max}}$ and J_{max}, scaled with photosynthetic leaf N content (N_{pa}, $gN\ m^{-2}$) (Eqn 6, 9). The relationship between the intracellular CO_2 concentration (C_i, Pa) and the stomatal conductance (g_s, $mmol\ m^{-2}\ s^{-1}$) was modeled according to Falge et al. [27] (Eqn 14–17). g_s can limit A_n and thereby modify the linearity of the photosynthetic capacities *vs* N_{pa} relationship [28]. An analytical method was used to couple A_n and g_s, leading to the calculation of A_n through a system of five equations and five unknowns [29,30] (Eqn 17). The daytime temperature dependence of $V_{C_{max}}$ and J_{max} was described following Medlyn et al. [31] (Eqn 12). Some studies have shown from a large dataset that the entropy terms of $V_{C_{max}}$ and J_{max} acclimate to the mean growth temperature (T_g, K) experienced by leaves over the preceding month [32]. The formalism and parameterization proposed by these authors [32] was used in this study to describe the acclimation of $V_{C_{max}}$ and J_{max} to T_g (Eqn 18–19). Similarly, Ainsworth and Long [33] have shown an acclimation of A_n to atmospheric CO_2 concentration during the preceding month (C_g, Pa). This was also taken into account (Eqn 20–21), by modifying the relationship of Vc_{max} and J_{max} at standard temperature (J_{fac}, dimensionless) and the relationship of Vc_{max} at standard temperature to N_{pa} (k_3, $\mu molCO_2\ g^{-1}\ N\ s^{-1}$) according to a linear function of the difference between reference (C_a^r) and growth CO_2 concentrations (C_g).

A sensitivity analysis of the photosynthesis-stomatal conductance model was performed by analyzing the range of parameter variations in literature (Text S1, Table S2) and the sensitivity of the model outputs in response to a ±15% change in parameter values (Text S1, Fig. S2–S3). An index of sensitivity (IOS) was calculated as the ratio of output to parameter changes and was used to discuss on the model uncertainties linked to model calibration.

Coordinated N Content of Sunlit Leaves

Within leaves, N is partitioned between metabolic and structural pools [24,25]. The coordinated leaf N content, N_{ac} ($gN\ m^{-2}$) is calculated as the sum of structural leaf N and of photosynthetic leaf N (Np_{ac}, $gN\ m^{-2}$). As leaf structures are highly dependent upon the biomass investment in dry matter (DM) [34], structural leaf N (f_{ns}, $gN\ g^{-1}$ DM) is expressed per unit DM. f_{ns} is assumed constant across species and independent of canopy depth and light intensity. f_{ns} value corresponds to the average value reported in the literature for a range of C_3 species (0.012 $gN\ g^{-1}$ DM, for a review see Lötscher et al. [25]). In contrast, metabolic leaf N associated with leaf photosynthesis is expressed per unit area since both light capture and CO_2 exchange with atmosphere are intrinsically area-based phenomena [3]. As a key measure of leaf morphology [6], SLA links dry matter-based structural N content (f_{ns}) to area-based photosynthetic N content (Np_{ac}):

$$N_{ac} = Np_{ac} + f_{ns}/SLA \tag{1}$$

Table 1. Equations of the photosynthesis - stomatal conductance models.

Process	Equation	Unit	Eqn	Ref.
Nitrogen sub-model				
Leaf nitrogen content	$N_{\mathrm{ac}} = Np_{\mathrm{ac}} + f_{\mathrm{ns}}/SLA$	g N m^{-2}	1	–
Leaf photosynthetic N content	$Np_{ac} = \frac{4 \cdot 1\alpha \cdot \mathrm{PPFD}}{k_3^{\mathrm{ac}}} \cdot \left(\left(\frac{\mathrm{C_i} + k_2}{(4 \cdot C_{\mathrm{i}} + 8 \cdot \Gamma^*) \cdot \Phi_{V_{\mathrm{cmax}}}} \right)^2 - \left(\frac{1}{J_{\mathrm{fac}}^{\mathrm{atc}} \cdot \Phi_{J_{\mathrm{max}}}} \right)^2 \right)^{1/2}$	g N m^{-2}	2	–
Photosynthetic sub-model				
Net photosynthetic rate	$A_{\mathrm{n}} = (1 - \Gamma * / C_{\mathrm{i}}) \cdot \min\{W_{\mathrm{c}}, W_{\mathrm{j}}\} - R_{\mathrm{day}}$	µmol m^{-2} s^{-1}	3	[1]
Rubisco limited photosynthetic rate through RuBP carboxylation/oxygenation	$W_{\mathrm{c}} = {}^{\mathrm{r}}_{\mathrm{C_{max}}} \cdot \Phi_{V_{\mathrm{cmax}}} \cdot \frac{C_{\mathrm{i}}}{C_{\mathrm{i}} + k_2}$	µmol m^{-2} s^{-1}	4	[1]
Intermediate variable synthesising the Rubisco affinity for CO$_2$	$k_2 = K_{\mathrm{c}} \cdot \Theta_{K_{\mathrm{c}}} \cdot (1 + O_{\mathrm{i}} / (K_{\mathrm{O}} \cdot \Theta_{K_{\mathrm{O}}}))$	Pa	5	[1]
Maximum rate of carboxylation	$V_{\mathrm{C_{max}}}^{\mathrm{r}} = k_3^{\mathrm{ac}} \cdot N_{\mathrm{pa}}$	µmol m^{-2} s^{-1}	6	[2]
RuBP regeneration limited photosyn¯thetic rate through electron transport	$W_{\mathrm{j}} = J \cdot \frac{Ci}{4 \cdot Ci + 8 \cdot \Gamma^*}$	µmol m^{-2} s^{-1}	7	[1]
Light dependence of electron transport rate	$J = \frac{4 \cdot \alpha \cdot PPFD}{\left(1 + (4 \cdot \alpha \cdot PPFD)^2 \big/ \left(J_{\mathrm{max}}^{\mathrm{r}} \cdot \Phi_{J_{\mathrm{max}}}\right)^2\right)^{1/2}}$	µmol m^{-2} s^{-1}	8	[1]
Potential RuBP regeneration rate	$J_{\mathrm{max}}^{\mathrm{r}} = J_{\mathrm{fac}}^{\mathrm{atc}} \cdot V_{\mathrm{C_{max}}}^{\mathrm{r}}$	µmol m^{-2} s^{-1}	9	[2]
CO$_2$ compensation point in the absence of mitochondrial respiration	$\Gamma^* = {}^{0.5 \cdot O_{\mathrm{i}}}\!/_{\tau \cdot \Theta_\tau}$	Pa	10	[1]
Leaf respiration without photorespiration	$R_{\mathrm{day}} = I_{\mathrm{fac}} \cdot R_{\mathrm{dark}}^{\mathrm{r}} \cdot \Theta_{R_{\mathrm{dark}}}$ $R_{\mathrm{dark}}^{\mathrm{r}} = R_{\mathrm{fac}} \cdot V_{\mathrm{C_{max}}}^{\mathrm{r}}$ $I_{\mathrm{fac}} = 0.5, \text{ if } PPFD > 25\ \mu mol\, m^{-2}\, s^{-1}$ $I_{\mathrm{fac}} = c \cdot PPFD + d, \text{ if } PPFD \leq 25\ \mu mol\, m^{-2}\, s^{-1}$	µmol m^{-2} s^{-1}	11	[27]
Temperature dependence of J_{max} and Vc_{max}	$\Phi = \exp\left[\frac{\Delta\mathrm{Ha}}{R \cdot T^{\mathrm{r}}} \cdot \left(1 - \frac{T^{\mathrm{r}}}{T_{\mathrm{K}}}\right)\right] \cdot \frac{1 + \exp\left[\frac{\Delta\mathrm{S}^{\mathrm{at}} \cdot T^{\mathrm{r}} - \Delta\mathrm{Hd}}{R \cdot T^{\mathrm{r}}}\right]}{1 + \exp\left[\frac{\Delta\mathrm{S}^{\mathrm{at}} \cdot T_{\mathrm{K}} - \Delta\mathrm{Hd}}{R \cdot T_{\mathrm{K}}}\right]}$	dimensionless	12	[31]
Temperature dependence of K_c, K_o, τ and R_{dark}	$\Theta = \exp\left[\frac{\Delta\mathrm{Ha}}{R \cdot T^{\mathrm{r}}} \cdot (1 - T^{\mathrm{r}}/T_{\mathrm{K}})\right]$	dimensionless	13	[27]
Stomatal conductance sub-model				
Stomatal conductance	$g_{\mathrm{s}} = g_{\mathrm{min}} + g_{\mathrm{fac}} \cdot (A_n + I_{\mathrm{fac}} \cdot R_{\mathrm{dark}}) \cdot 10^2 \cdot h_{\mathrm{s}} / C_{\mathrm{s}}$	mmol m^{-2} s^{-1}	14	[27]
CO$_2$ partial pressure at the leaf boundary layer	$C_{\mathrm{s}} = C_{\mathrm{a}} - A_{\mathrm{n}} \cdot 10^2 / g_{\mathrm{b}}$	Pa	15	[3]
Photosynthesis-stomata coupling				
CO$_2$ intercellular concentration	$C_{\mathrm{i}} = C_{\mathrm{s}} - A_{\mathrm{n}} \cdot 1.6 \cdot 10^2 / g_{\mathrm{s}}$	Pa	16	[29]
Analytical solution for photosynthesis calculation	$A = \frac{a \cdot C_{\mathrm{i}} - a \cdot d}{e \cdot C_{\mathrm{i}} + b} - R_{\mathrm{day}}$ $e \cdot \alpha \cdot A_{\mathrm{n}}^3 + A_{\mathrm{n}}^2 \cdot (e \cdot \beta + b \cdot \theta + e \cdot \alpha \cdot R_{day} - a \cdot \alpha)$ $+ A_n \cdot \left(e \cdot \gamma + b \cdot \frac{\gamma}{C_{\mathrm{a}}} + e \cdot \beta \cdot R_{\mathrm{day}} + b \cdot \theta \cdot R_{\mathrm{day}} - a \cdot \beta + a \cdot d \cdot \theta\right)$ $+ \left(e \cdot \gamma \cdot R_{\mathrm{day}} + b \cdot R_{\mathrm{day}} \cdot \frac{\gamma}{C_{\mathrm{a}}} - a \cdot \gamma + a \cdot d \cdot \frac{\gamma}{C_{\mathrm{a}}}\right) = 0$ $\alpha = g_{\mathrm{min}} / g_{\mathrm{b}} - g_{\mathrm{fac}} \cdot h_{\mathrm{s}} \cdot 10^2 + 1.6 \cdot 10^2$ $\beta = C_{\mathrm{a}} \cdot (g_{\mathrm{b}} \cdot g_{\mathrm{fac}} \cdot h_{\mathrm{s}} - 2 \cdot g_{\mathrm{min}} - 1.6 \cdot g_{\mathrm{b}}) - R_{\mathrm{day}} \cdot g_{\mathrm{fac}} \cdot h_{\mathrm{s}} \cdot 10^2$ $\gamma = C_{\mathrm{a}} \cdot (C_{\mathrm{a}} \cdot g_{\mathrm{min}} \cdot g_{\mathrm{b}} \cdot 10^{-2} + R_{\mathrm{day}} \cdot g_{\mathrm{fac}} \cdot g_{\mathrm{b}} \cdot h_{\mathrm{s}})$ $\theta = g_{\mathrm{fac}} \cdot g_{\mathrm{b}} \cdot h_{\mathrm{s}} - g_{\mathrm{min}}$	µmol m^{-2} s^{-1}	17	[29]
Photosynthetic acclimation				
$\Delta S_{V_{\mathrm{cmax}}}^{\mathrm{at}} = \Delta S_{V_{\mathrm{cmax}}}^{r} + p_4 \cdot (T^{\mathrm{r}} - T_{\mathrm{g}})$ Photosynthetic $\Delta S_{J_{\mathrm{max}}}^{\mathrm{at}} = \Delta S_{J_{\mathrm{max}}}^{\mathrm{r}} + p_4 \cdot (T^{\mathrm{r}} - T_{\mathrm{g}})$ acclimation to growth temperature	$J_{\mathrm{fac}}^{\mathrm{at}} = J_{\mathrm{fac}} + p_1 \cdot (T^{\mathrm{r}} - T_{\mathrm{g}})$	J K^{-1} mol^{-1} J K^{-1} mol^{-1} dimensionless	18a 18b 19	[32]
Photosynthetic acclimation to CO$_2$ concentration	$J_{\mathrm{fac}}^{\mathrm{ac}} = J_{\mathrm{fac}}^{r} + p_2 \cdot (C_{\mathrm{a}}^{\mathrm{r}} - C_{\mathrm{g}})$ $k_3^{\mathrm{ac}} = k_3^{\mathrm{r}} + p_3 \cdot (C_{\mathrm{a}}^{\mathrm{r}} - C_{\mathrm{g}})$	dimensionless µmol g^{-1} N s^{-1}	20 21	[33]

doi:10.1371/journal.pone.0038345.t001

Under given environmental conditions, Np_{ac} is defined as the N_{pa} value at which A_{n} was co-limited by W_{c} and W_{j} (Fig. S1). Both $V_{\mathrm{C_{max}}}$and J_{max} are linear functions of Np_{a} and, for given environmental conditions, there is a single Np_{ac} value for which W_{c} equals W_{j}. At this co-limiting point, Np_{ac} equals (see Text S2 Eqn 2a-2d for details):

Table 2. Parameters and variables of the photosynthesis - stomatal conductance models.

Symbol	Value	Unit	Description
Parameters			
C	−0.02	$m^2\ s\ \mu mol^{-1}$	Slope of the linear relationship between l_{fac} and *PPFD* in the range 0–25 $\mu mol\ m^{-2}\ s^{-1}$
C_a^r	35	Pa	Reference atmospheric CO_2 partial pressure
d	1	$\mu mol\ CO_2\ m^{-2}$ leaf s^{-1}	y-intercept of the linear relationship between l_{fac} and *PPFD* in the range from 0–25 $\mu mol\ m^{-2}\ s^{-1}$
g_b	300	$mmol\ m^{-2}\ s^{-1}$	Leaf boundary layer conductance to water vapour
g_{fac}	13.7	dimensionless	Stomatal sensitivity coefficient
g_{min}	76.2	$mmol\ m^{-2}\ s^{-1}$	Minimum stomatal conductance to water vapour
l_{fac}	0.5	dimensionless	Coefficient representing the extent to which R_{dark} is inhibited in the light
J_{fac}^r		dimensionless	Ratio between J_{max} and $V_{C_{max}}$ of plant grown at the reference temperature and at the reference CO_2 partial pressure
k_3^r		$\mu mol\ CO_2\ g^{-1}\ N\ s^{-1}$	Slope of linear relationship relating N_{pa} to $V_{C_{max}}$ at the reference temperature and at the reference CO_2 partial pressure
K_c	19.42	Pa	Michaelis-Menten constant for carboxylase activity of Rubisco
K_o	14 300	Pa	Michaelis-Menten constant for oxgenase activity of Rubisco
O_i	21 000	Pa	Internal leaf oxygen concentration
p_1	−0.012	dimensionless	Coefficient representing the extent to which J_{fac} is modified by the CO_2 partial pressure during plant growth
p_2	0.036	dimensionless	Coefficient representing the extent to which J_{fac} is modified by the temperature during plant growth
p_3	0.3192	$\mu mol\ CO_2\ g^{-1}\ N\ s^{-1}$	Coefficient representing the effect of CO_2 partial pressure during plant growth on k_3
p_4	0.94	dimensionless	Coefficient representing the effect of growth temperature on entropy term for J_{max} and $V_{C_{max}}$
R	8.314	$J\ K^{-1}\ mol^{-1}$	Perfect gas constant
R_{fac}	0.011	dimensionless	Ratio between R_{dark} and $V_{C_{max}}$ at reference temperature
SLA		m^2 leaf g^{-1} DM	Specific leaf area
α	0.05	mol CO_2 mol^{-1} photon	Apparent quantum yield of net photosynthesis at saturating CO_2
ΔHa_{Jmax}	83 608	$J\ mol^{-1}$	Activation energy of J_{max}
ΔHa_{Kc}	65 800	$J\ mol^{-1}$	Activation energy of K_c
ΔHa_{Ko}	36 000	$J\ mol^{-1}$	Activation energy of K_o
ΔHa_{Rdark}	50 861	$J\ mol^{-1}$	Activation energy of R_{dark}
ΔHa_{Vcmax}	86 529	$J\ mol^{-1}$	Activation energy of $V_{C_{max}}$
ΔHa_{τ}	−28 990	$J\ mol^{-1}$	Activation energy of τ
ΔHd	200 000	$J\ mol^{-1}$	Deactivation energy
$\Delta S_{J_{max}}^r$	660.42	$J\ K^{-1}\ mol^{-1}$	Entropy term of J_{max} for plant grown at reference temperature
$\Delta S_{V_{cmax}}^r$	654.24	$J\ K^{-1}\ mol^{-1}$	Entropy term of $V_{C_{max}}$ for plant grown at reference temperature
τ	2 838	dimensionless	Rubisco specificity factor at reference temperature
Input Variables			
C_a		Pa	CO_2 partial pressure in the ambient air
C_g		Pa	Atmospheric CO_2 partial pressure during preceding month of plant growth
h_s		dimensionless	Leaf surface relative humidity
PPFD		$\mu mol\ m^{-2}\ s^{-1}$	Photosynthetic photon flux density
T_k		K	Air temperature. In our analysis $T_k = T_g$
T_g		K	Mean air temperature during preceding month of plant growth
T^r	293.16	K	Reference temperature for metabolic activity
Output variables			
A_n		$\mu mol\ m^{-2}\ s^{-1}$	Net photosynthesis
C_i		Pa	Internal CO_2 partial pressure
C_s		Pa	Leaf surface CO_2 partial pressure
g_s		$mmol\ m^{-2}\ s^{-1}$	Stomatal conductance to water vapor
k_2		Pa	Intermediate variable synthesizing the Rubisco affinity for CO_2
J		$\mu mol\ m^{-2}\ s^{-1}$	Light dependence of the rate of electron transport

Table 2. Cont.

Symbol	Value	Unit	Description
$J_{\mathrm{fac}}^{\mathrm{ac}}$		dimensionless	J_{fac} acclimated to CO_2 during plant growth
$J_{\mathrm{fac}}^{\mathrm{at}}$		dimensionless	J_{fac} acclimated to temperature during plant growth
$J_{\mathrm{fac}}^{\mathrm{atc}}$		dimensionless	J_{fac} acclimated to CO_2 and to temperature during plant growth
J_{max}		μmol m^{-2} s^{-1}	Potential rate of RuBP regeneration
$J_{\mathrm{max}}^{\mathrm{r}}$		μmol m^{-2} s^{-1}	Potential rate of RuBP regeneration at reference temperature
k_3		μmol CO_2 g^{-1} N s^{-1}	Slope of linear relationship relating N_{pa} to $V_{\mathrm{C_{max}}}$
k_3^{ac}		μmol CO_2 g^{-1} N s^{-1}	Slope of linear relationship relating N_{pa} to $V_{\mathrm{C_{max}}}$ acclimated to CO_2 during plant growth
N_{a}		g N m^{-2} leaf	Leaf N content per leaf area
N_{ac}		g N m^{-2} leaf	Leaf N content per leaf area when W_{c} equals W_{j}
N_{pa}		g N m^{-2} leaf	Leaf photosynthetic N content per leaf area
Np_{ac}		g N m^{-2} leaf	Leaf photosynthetic N content per leaf area when W_{c} equals W_{j}
R_{dark}		μmol m^{-2} s^{-1}	Leaf dark respiration rate
$R_{\mathrm{dark}}^{\mathrm{r}}$		μmol m^{-2} s^{-1}	Leaf dark respiration rate at reference temperature
R_{day}		μmol m^{-2} s^{-1}	Leaf respiration rate from processes other than photorespiration
$V_{\mathrm{C_{max}}}$		μmol m^{-2} s^{-1}	Maximum carboxylation rate of Rubisco
$V_{\mathrm{C_{max}}}^{\mathrm{r}}$		μmol m^{-2} s^{-1}	Maximum carboxylation rate of Rubisco at reference temperature in the absence of any deactivation as a result of high temperature
W_{c}		μmol m^{-2} s^{-1}	Rubisco-limited photosynthetic rate
W_{j}		μmol m^{-2} s^{-1}	RuBP regeneration limited photosynthetic rate through electron transport
Φ		dimensionless	Temperature dependence of J_{max} or $V_{\mathrm{C_{max}}}$
$\Phi_{V_{\mathrm{cmax}}}$		dimensionless	Temperature dependence of $V_{\mathrm{C_{max}}}$
$\Phi_{J_{\mathrm{max}}}$		dimensionless	Temperature dependence of J_{max}
Θ		dimensionless	Temperature dependence of K_c, K_o, τ, or R_{dark}
$\Theta_{K_{\mathrm{c}}}$		dimensionless	Temperature dependence of K_{c}
$\Theta_{K_{\mathrm{o}}}$		dimensionless	Temperature dependence of K_{o}
Θ_{τ}		dimensionless	Temperature dependence of τ
$\Theta_{R_{\mathrm{dark}}}$		dimensionless	Temperature dependence of R_{dark}
Γ^*		dimensionless	CO_2 compensation point in the absence of mitochondrial respiration
ΔS^{at}		J K^{-1} mol^{-1}	Entropy term acclimated to temperature during plant growth
$\Delta S_{J_{\mathrm{max}}}^{\mathrm{at}}$		J K^{-1} mol^{-1}	Entropy term of J_{max} acclimated to temperature during plant growth
$\Delta S_{V_{\mathrm{cmax}}}^{\mathrm{at}}$		J K^{-1} mol^{-1}	Entropy term of $V_{\mathrm{C_{max}}}$ acclimated to temperature during plant growth

Parameter values are derived from Wohlfahrt et al. [3–4].
doi:10.1371/journal.pone.0038345.t002

$$Np_{ac} = \frac{4\cdot 1\alpha\cdot \mathrm{PPFD}}{k_3^{\mathrm{ac}}}\cdot \left(\left(\frac{\mathrm{C_i}+k_2}{(4\cdot C_{\mathrm{i}}+8\cdot\Gamma^*)\cdot\Phi_{V_{\mathrm{Cmax}}}}\right)^2-\left(\frac{1}{J_{\mathrm{fac}}^{\mathrm{atc}}\cdot\Phi_{J_{\mathrm{max}}}}\right)^2\right)^{1/2} \qquad (2)$$

where α (molCO$_2$ mol^{-1}photon) is the apparent quantum yield of A_{n} at saturating CO_2, *PPFD* (μmol m^{-2} s^{-1}) is the photosynthetic photon flux density, k_3^{ac}(μmol CO_2 g^{-1}N s^{-1}) is k_3 acclimated to C_{g} (Eqn 21), k_2 (Pa) is an intermediate variable synthesizing the Rubisco affinity for CO_2 (Eqn 5), Γ^* (Pa) is the CO_2 compensation point in the absence of mitochondrial respiration, $J_{\mathrm{fac}}^{\mathrm{atc}}$ is J_{fac} acclimated to C_{g} and T_{g} (CO_2 air concentration and temperature during preceding month of plant growth, Eqn 19–20), and $\Phi_{V_{\mathrm{Cmax}}}$ and $\Phi_{J_{\mathrm{max}}}$ (dimensionless) are the response functions of V_{Cmax} and J_{max} to temperature (Eqn 12). Overall, Np_{ac} integrates the sensitivity of photosynthetic machinery to T_{g}, *PPFD*, C_{i} and h_{s}.

Dataset

A dataset was assembled from measurements and literature to associate leaf photosynthetic traits of mature sunlit leaves with environmental growth conditions (Dataset SI4). $V_{\mathrm{C_{max}}}$ and J_{max} at reference temperature ($T^{\mathrm{r}}=20°\mathrm{C}$), N_{a}, *SLA*, as well as T_{g}, *PPFD*, h_{s} and C_{g} during the month preceding leaf measurements were included. $V_{\mathrm{C_{max}}}$ and J_{max} values were standardized using a consistent formulation and parameterization of Γ^* and the Michaelis-Menten constants for carboxylase (K_{c}, Pa) and oxygenase (K_{o}, Pa) Rubisco activity [32,35].

The dataset has 293 entries from 31 C_3 plant species covering six plant functional types (PFTs): temperate broadleaved and coniferous evergreen trees (PFT1), temperate broadleaved deciduous trees (PFT2), deciduous shrubs and herbs (PFT3), perennial C_3 grasses and forbs (PFT4), C_3 crops (wheat, PFT5) and N-fixing trees (PFT6). The final dataset covers a wide range of plant growth conditions: T_g (ranging from 7.1 to 21.0°C), *PPFD* (500 to 1170 μmol m^{-2} s^{-1}), h_s (0.51 to 0.89) and C_g (36 and 60 Pa). However, data corresponding to severe drought and/or to very low N availability during growth were excluded from the dataset. Four categories of inorganic N availability (low, medium, high and very high), two categories of soil moisture and of atmospheric CO_2 concentration (ambient and elevated) and six categories of experimental set-up (climate chamber, sunlit climate chamber, botanical garden, natural vegetation, free air CO_2 enrichment (FACE) and open top chambers) were defined. The dataset has been made available via the TRY initiative on plant traits [36].

Data Analysis

Coordinated W_c and W_j. The basic assumption of the coordination hypothesis is that under the environmental conditions to which a leaf is adapted, RuBP carboxylation equals RuBP regeneration ($W_c = W_j$). Here we tested this for the average daily plant growth conditions (excluding night values) during the last month preceding photosynthesis measurements. We used four environmental variables (C_g, *PPFD*, T_g and h_s) corresponding to the average plant growth conditions as model input, and $V_{C_{max}}$ and J_{max} derived from separate photosynthesis measurements on the same plants. A single set of values was used for all other 33 model parameters and was originated from Wohlfahrt's calibration (Table 2) [3,4]. W_c and W_j, both predicted for the average plant growth conditions for each observation (n = 293), were compared by least square linear regression. Regression residuals were analyzed using a general linear model (GLM) with T_g, h_s, C_g and with PFTs and N categories. PFTs and N levels were compared by the post ANOVA Tukey's HSD method.

Prediction of the coordinated leaf N content. N_{ac} was calculated for each observation (n = 293) using four environmental variables (C_g, *PPFD*, T_g and h_s) corresponding to the growth conditions of the past month and three leaf traits (k_3, J_{fac} and *SLA*). k_3 is calculated as the ratio between $V_{C_{max}}$ and Np_a, while J_{fac} is calculated as the ratio between J_{max} and $V_{C_{max}}$. The prediction of N_{ac} was evaluated by the relative root mean squared error (RRMSE), which is the relative average of the squared differences between predicted and observed values [37]. RRMSE values lower than 0.2 indicates here acceptable errors. Systematic ($RRMSE_S$) and unsystematic ($RRMSE_U$) errors [37] specified the error source of RRMSE (Eq. I).

$$RRMSE_S = \left[\sum_{i=1}^{n} \left(\hat{E}_i - M_i \right)^2 \Big/ n \right]^{0.5} \cdot \frac{1}{\bar{M}} \quad with\ \hat{E}_i = b \cdot M_i + a \tag{I}$$

$$RRMSE_U = \left[\sum_{i=1}^{n} \left(E_i - \hat{E}_i \right)^2 \Big/ n \right]^{0.5} \cdot \frac{1}{\bar{M}}$$

where E_i and M_i are the predicted and measured values of the observation *i*, $\bar{M}_i$ is the average of M_i and $\hat{E}_i$ is an estimate of E_i deriving from the linear regression between E_i and M_i.

Dependence of leaf photosynthetic parameters on plant functional type (PFT). ANOVA followed by LSD method for mean comparison tests, were used to analyze the role of PFT for the estimation of leaf photosynthetic traits used in the test of the coordination hypothesis ($V_{C_{max}}$, J_{max}, k_3, J_{fac} and *SLA*). In order to test if the calibration of leaf photosynthetic traits can be simplified to obtain a unique value or a value by PFT, we estimated independent values of k_3, J_{fac} and *SLA* traits minimizing the squared differences between N_a and N_{ac} (Newton's optimization method). Mean and optimized values per PFT were then compared by linear regressions. The calibration of leaf traits by species was not tested since the number of observations per species was too variable in our dataset.

Dependence of leaf photosynthetic parameters on environmental growth conditions. Multiple regression models were used to analyze the effects of environmental growth conditions (T_g, *PPFD*, h_s and C_g, N and soil moisture categories) on leaf traits ($V_{C_{max}}$, J_{max}, k_3, J_{fac} and *SLA*). For regression models of k_3 and J_{fac}, the values of dependent variables were log-transformed and all residuals followed a normal distribution.

We tested if the prediction of leaf photosynthetic traits by environmental growth conditions was robust and validated likewise the coordination hypothesis. We conducted bootstrap analyses to predict W_c and W_j as a function of $V_{C_{max}}$ and J_{max} estimated by an independent regression model and environmental growth conditions. In the same way, bootstrap analyses were conducted to predict N_{ac} as a function of estimated k_3 and J_{fac}. To do so, two-thirds of the 293 observations were randomly used to parameterize the multiple regression models (20 random sets, Tables S3–S4). These models were used to predict the leaf photosynthetic parameters $V_{C_{max}}$, J_{max}, k_3 and J_{fac} of the remaining observations from their environmental growth conditions. As *SLA* was not predictable from environmental growth conditions (see in result the low coefficient of determination in *SLA* regression model), experimental specific values were used. Finally, W_c, W_j and N_{ac} were calculated and the coordination hypothesis was evaluated again (Tables S5–S6).

We also attempted to falsify the testable hypothesis ($W_c = W_j$ and $N_a = N_{ac}$) provided by the photosynthetic coordination hypothesis. To this end, we randomized environmental growth conditions among observations (permutation test) and tested the alternative hypothesis significant differences between W_c and W_j and between N_a and N_{ac}.

Prediction from our leaf photosynthesis coordination model. The implications of the coordination hypothesis for N_{ac}, A_n and *PNUE* were tested by varying: i) the values of the leaf parameters k_3 and J_{fac} under mean environmental growth conditions (*PPFD* = 666 μmol m^{-2} s^{-1}, $T_g = 16.9$°C, $h_s = 0.74$); ii) the values of the environmental growth parameters T_g and *PPFD* assuming mean leaf photosynthetic parameter values ($k_3 = 59.1$ μmol $g^{-1}$$Np_a$ s^{-1}; $J_{fac} = 2.45$; *SLA* = 17.7 m^2 kg^{-1} DM).

All statistical tests were performed using Statgraphics Plus (v. 4.1, Manugistics, USA).

Results

Leaf Photosynthesis Shows Co-limitation Under Mean Growth Conditions

We assessed the level of photosynthetic co-limitation by comparing dark (W_c) to light-driven (W_j) biochemical processes under growth conditions experienced by the leaves in the month prior to observations. W_c strongly correlated with W_j (Fig. 1A, n = 293, $P<0.001$, intercept not significantly different from zero) across species and growth environments (characterized by T_g, *PPFD*, h_s and C_g). An ANOVA on the regression residuals revealed a significant PFT effect (*d.f.* = 5, 283; $P<0.001$; data not shown). The calculated W_c/W_j ratio was not significantly different from one (*t*-test at $P<0.05$, n = 293). This ratio varied neither with species parameters, nor with environmental growth conditions.

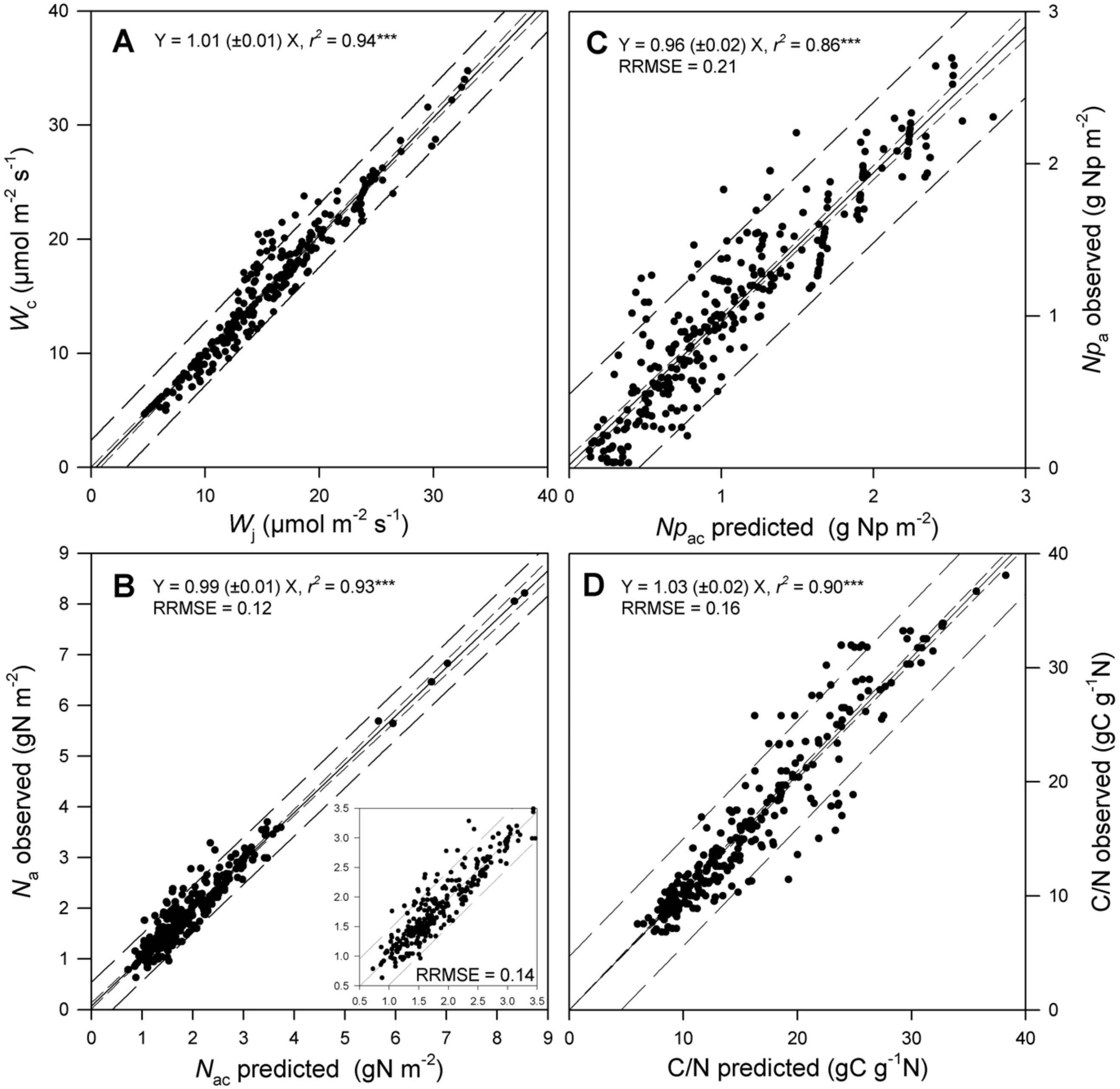

Figure 1. Tests of the coordination hypothesis using experimental values of leaf photosynthetic traits (*Vc_{max}*, *J_{max}*, *J_{fac}*, *k_3* and *SLA*). A) Relationship between the predicted rates of RuBP carboxylation/oxygenation (W_c) and RuBP regeneration (W_j) under plant growth conditions. B) Relationship between predicted (N_{ac}) and observed (N_a) leaf N content. N_a was calculated as the sum of the leaf photosynthetic and structural N contents. Leaf photosynthetic N content was predicted using Eqn 2 with the species-specific parameters k_3 and J_{fac}. C) Relationship between predicted (Np_{ac}) and observed (Np_a) photosynthetic leaf N content. D) Relationship between predicted and observed leaf C/N ratio. A common leaf structural N content was used (fns =0.012 gN g^{-1} DM). Solid lines are the regressions. Short-dashed and long-dashed lines indicate the confidence (at 95%) and prediction intervals, respectively. The insert in Fig. 1B shows the same relationship without the very high observed N_a values for the PFT1. ***, $P<0.001$.
doi:10.1371/journal.pone.0038345.g001

Predicted Coordinated Leaf N Content (N_{ac}) Matches Observed Leaf N Content (N_a)

Overall, predicted and observed N_a values were closely correlated with a slope not significantly different from one and an intercept not significantly different from zero (Fig. 1B, n = 293, $P<0.001$, RRMSE =0.12). The breakdown of RRMSE into unsystematic and systematic error terms showed that the prediction error was mostly unsystematic and therefore associated to data and not to a systematic model error (RRMSEs =0.012; RRMSEu =0.108). An ANOVA on the residuals of the prediction showed weak but significant effects of PFTs, T_g and h_s (*d.f.* =5, 1, 1, respectively; $P<0.01$; data not shown).

As f_{ns} was assumed constant across species [25], we calculated N_{pa} and N_{pac} by subtracting the ratio f_{ns}/SLA to N_a and N_{ac}, respectively. Similarly, predicted and observed Np_a values were closely correlated (Fig. 1C, n = 293, $P<0.001$, RRMSE =0.21).

Table 3. Estimates of the optimized value (for the entire dataset and by PFT) of leaf photosynthetic traits (J_{fac}, k_3 and SLA).

A)	**Optimized value**	W_c/W_j		N_a/N_{ac}		
Parameter		**Slope**	r^2	**Slope**	r^2	**RRMSE**
k_3						
All	48.3	1.15±0.02	0.78	0.94±0.02	0.64	0.28
PFT	45.2; 37.1; 54.0; 79.4; 46.2; 24.2	1.08±0.02	0.88	0.96±0.02	0.73	0.23
J_{fac}						
All	2.11	1.06±0.02	0.89	0.97±0.02	0.68	0.31
PFT	2.11; 2.11; 2.59; 1.70; 2.33; 3.10	1.04±0.02	0.92	1.02±0.02	0.79	0.23
SLA						
All	17.7	1.02±0.02	0.92.	0.88±0.02	0.43	0.44
PFT	8.1; 13.7; 18.2; 20.0; 18.3; 13.4	1.02±0.02	0.92.	0.96±0.02	0.48	0.37
k_3 and J_{fac}						
All	$k_3 = 48.3$; $J_{fac} = 2.11$	1.18±0.02	0.79	0.89±0.02	0.68	0.33
PFT	$k_3 = 45.2$; 37.1; 54.0; 79.4; 46.2; 24.2 $J_{fac} = 2.11$; 2.11; 2.59; 1.70; 2.33; 3.10	1.06±0.02	0.88	0.96±0.02	0.74	0.26

B)	k_3		J_{fac}		SLA	
PFT	**Mean**	**Optimized**	**Mean**	**Optimized**	**Mean**	**Optimized**
PFT1	65.0	45.2	2.23	2.11	11.1	8.1
PFT2	46.6	37.1	2.32	2.11	13.1	13.7
PFT3	90.1	54.0	2.53	2.59	21.4	18.2
PFT4	86.1	79.4	2.04	1.7	22.0	20.0
PFT5	44.9	46.2	2.69	2.33	18.3	18.3
PFT6	38.1	24.2	2.50	3.1	20.3	13.4
Correlation	$r^2 = 0.68$	$P<0.001$	$r^2 = 0.49$	$P<0.001$	$r^2 = 0.68$	$P<0.001$

The squared difference between measured N_a and predicted N_{ac} values were minimized by Newton's method. A) The optimization was done with one trait at a time without changing the values of the two other traits. The optimized values are ordered by PFT (i.e. the first value corresponds to PFT1). B) The optimized values by PFT were compared to mean per PFT in the dataset by using a linear regression model. Abbreviations: PFT1, temperate broadleaved and coniferous evergreen trees; PFT2, temperate broadleaved deciduous trees; PFT3, deciduous shrubs and herbs; PFT4, perennial C_3 grasses and forbs; PFT5, C_3 crops (wheat); PFT6, N-fixing trees.

doi:10.1371/journal.pone.0038345.t003

As carbon content in leaves was assumed to be approximately constant, we calculated a C/N ratio by dividing N_a and N_{ac} by the ratio between a common carbon content ($fcs = 0.45$ gC g^{-1} DM; [36,38]) and SLA. Predicted C/N matched significantly the calculated C/N, observed across environmental conditions and across species and PFTs (Fig. 1D).

Dependency of Leaf Parameters on Plant Functional Type

In the dataset (Table S1), the parameters used to calculate leaf photosynthesis and stomatal conductance were SLA, J_{fac}, k_3, calculated from $V_{C_{max}}$, J_{max} and leaf N measurements (Eqn 12, 15). At T^r, $V_{C_{max}}$ and J_{max} varied between 4–141 µmol m^{-2} s^{-1} and 8–213 µmol m^{-2} s^{-1}, respectively. k_3 varied from 4.6 to 350 µmol g^{-1}N s^{-1} while J_{fac} values were very constrained from 1.69 to 3.71, as already observed [2]. Finally, SLA varied from 1.5 to 43.2 m^2 kg^{-1} DM. All photosynthetic traits showed significant dependency to PFT ($P<0.001$) but with different determination coefficient ($r^2 = 0.66$, 0.64, 0.24, 0.47 and 0.40 for $V_{C_{max}}$, J_{max}, k_3, J_{fac} and SLA, respectively). Post-ANOVA LSD tests showed that the discrimination among the PFTs was more effective for J_{fac}, J_{max} and SLA separating significantly four groups among the six PFTs (Table S7) and was much weaker for k_3 and $V_{C_{max}}$ (two groups were significantly distinguished).

k_3, J_{fac} and SLA can be optimized to a value which minimizes the squared differences between N_a and N_{ac} (Table 3A). When k_3 was optimized by PFT, N_a was accurately predicted (slope $= 0.96$, $r^2 = 0.73$, RRMSE $= 0.23$). When a single value was used for the whole dataset, N_a prediction was not satisfactory. The optimization by PFT of J_{fac} led to a strong prediction of N_a (slope not different from one, $r^2 = 0.79$, RRMSE $= 0.23$). When a single value was used for the entire dataset ($J_{fac} = 2.11$), the prediction of N_a was less accurate but the slope of the relationship between W_c and W_j remained close to one. Finally, the optimisation of SLA by PFT or to a single value for the entire dataset strongly reduced the accuracy of N_a prediction. Optimization of the k_3 and J_{fac} parameters showed that N_a can be acceptably predicted when their values are defined by PFT. For all traits, average values by PFT and optimized values by PFT displayed significant linear relationships (Table 3B).

Table 4. Effects of environmental conditions on the leaf photosynthetic traits: $V_{C_{max}}$ J_{max}, J_{fac}, k_3 and *SLA*.

A)		J_{max}		$V_{C_{max}}$		**log** J_{fac}		**log** k_3		*SLA*	
Factors	**d.f.**	**Variance**	***P*-value**	**Variance**	***P*-value**	**Variance**	***P*-value**	**Variance**	***P*-value**	**Variance**	***P*-value**
CO_2 level	1	.	ns	4.6	<0.01	27.0	<0.001	.	ns	.	ns
N level	3	35.5	<0.001	24.5	<0.001	9.8	<0.05	65.1	<0.001	7.3	<0.05
H_2O level	1	12.2	<0.001	15.3	<0.001	8.1	<0.01	.	ns	3.1	<0.01
PPFD	1	6.6	<0.01	8.9	<0.001	5.7	<0.05	2.1	<0.05	0.1	<0.01
T_g	1	9.5	<0.01	33.1	<0.001	.	ns	25.3	<0.001	77.9	<0.001
h_s	1	12.7	<0.001	5.4	<0.01	19.2	<0.001	4.5	<0.01	1.8	<0.05
*PPFD**T_g	1	5.4	<0.05	.	ns	6.0	<0.05	.	ns	.	ns
*PPFD**h_s	1	18.1	<0.001	8.2	<0.001	24.2	<0.001	3.0	<0.05	9.7	<0.05
Overall	293	$r^2=0.64$	<0.001	$r^2=0.66$	<0.001	$r^2=0.51$	<0.001	$r^2=0.44$	<0.001	$r^2=0.15$	<0.01

B)	J_{max}		$V_{C_{max}}$		**log** J_{fac}		**log** k_3		*SLA*	
Factors	**Estimate**	**Error**	**Estimate**	**Error**	**Estimate**	**Error**	**Estimate**	**Error**	**Estimate**	**Error**
Constant	−2.1	12	−19.0	42	62.7 E−03	257.0 E−03	2.53	1.06	54.0	15.3
CO_2	ns	ns	−8.2	3.1	84.4 E−03	17.4 E−03	ns	ns	ns	ns
N	10.4	3.3	4.1	1.2	−4.4 E−03	6.8 E−03	−0.29	0.03	0.95	0.42
H_2O	−43.2	13.0	−17.8	4.0	−65.2 E−03	26.7 E−03	ns	ns	4.1	1.4
PPFD	0.58	0.16	0.24	0.05	0.93 E−03	0.33 E−03	2.77 E−03	1.37 E−03	−0.05	0.02
T_g	−21.3	7.0	−3.0	0.4	ns	ns	−59.9 E−03	6.76 E−03	−0.83	0.13
h_s	784	181	210	57	1.64	0.38	4.33	1.41	−41.6	20.9
*PPFD**T_g	0.018	0.008	ns	ns	3.62 E−05	1.75 E−05	ns	ns	ns	ns
*PPFD**h_s	−1.21	0.24	−0.31	0.07	−2.4 E−03	0.5 E−03	−4.01 E−03	1.81 E−03	0.06	0.03

The factors are environmental growth conditions: radiation (*PPFD*), temperature (T_g), relative humidity (h_s), air CO_2 concentration (CO_2 level), soil N availability (N level) and soil moisture (H_2O level). A) Degree of freedom (*d.f.*), variance explained (%), statistical significance and sign (positive or negative) of interactions with continuous variables. B) Coefficients estimate of ANOVA model. All variable values were analyzed at a reference temperature of 20°C. Residuals of analysis followed a normal distribution without transformation for $V_{C_{max}}$ and J_{max}, and with log-transformation for J_{fac} and k_3. We only included in the ANOVA model the interactions that were significant.

doi:10.1371/journal.pone.0038345.t004

Dependency of Leaf Parameters to Environmental Growth Conditions

All leaf photosynthetic parameters could be predicted from environmental growth conditions (Table 4). However, *SLA* was poorly correlated with environmental conditions ($r^2=0.15$). J_{max} was reasonably well predicted by environment ($r^2=0.64$, $P<0.001$). It was predominantly affected by the N level experienced by plants during growth (36% of explained variance), with a high N level leading to higher J_{max} values. J_{max} was then positively affected by *PPFD* (7%), h_s (13%), and *PPFD* times T_g (5%) and was negatively affected by soil moisture level (12%), T_g (9%), and *PPFD* times h_s (18%). $V_{C_{max}}$, which was significantly predicted from environmental condition during growth ($r^2=0.66$, $P<0.001$), was mainly affected by T_g (33%, negatively), N level (25%, positively) and soil moisture level (15%, negatively). Then, $V_{C_{max}}$ was positively affected by *PPFD* (8%) and h_s (5%) and was negatively affected by CO_2 level (5%) and *PPFD* times h_s (8%).

J_{fac} was significantly predicted from environment ($r^2=0.51$, $P<0.001$) and the variance was shared between CO_2 level (27%, positively), h_s (19%, positively), and *PPFD* times h_s (24%, negatively). Note that J_{fac} increased with CO_2 concentration as reviewed by Ainsworth and Long [33]. The remaining variance was positively explained by *PPFD* (6%) and *PPFD* times T_g (6%) and negatively explained by N and moisture levels (10 and 8%, respectively). k_3 was significantly predicted ($r^2=0.44$, $P<0.001$) and the variance was predominantly explained by N level (65%), with higher k_3 at lower N availability level, as also reviewed by Ainsworth and Long [33]. The temperature experienced by leaves during the preceding month was also an important driver of k_3 (25%), with lower k_3 at higher temperature. The remaining variance was positively explained by *PPFD* (2%) and h_s (4%) and negatively explained by *PPFD* times h_s (3%).

Once the multiple regression models were established for each leaf photosynthetic parameter, we tested by bootstrap analysis if their prediction was robust enough to satisfy the coordination hypothesis. All random datasets generated by bootstrap (n = 220) gave significant regression models (Tables S5–S6). The parameters values of these regression models were used with the remainder of the data (n = 293−220 = 70) to predict leaf photosynthetic parameters values. Photosynthetic parameters values were then used to predict W_c, W_j and N_{ac}. We found that W_c matched W_j (Fig. 2A) and N_{ac} matched N_a (Fig. 2B, RRMSE = 0.2), whatever the random dataset to which it was applied (Tables S5–S6).

In an attempt to falsify the leaf photosynthesis coordination hypothesis, we have randomized environmental growth conditions among observations. This randomization resulted in a strong mismatch between W_c and W_j (RRMSE = 0.76; slope $=0.60\pm0.33$; $r^2=13\%$) as well as between N_a and N_{ac} (RRMSE = 0.72; slope $=0.80\pm0.40$; $r^2=17\%$).

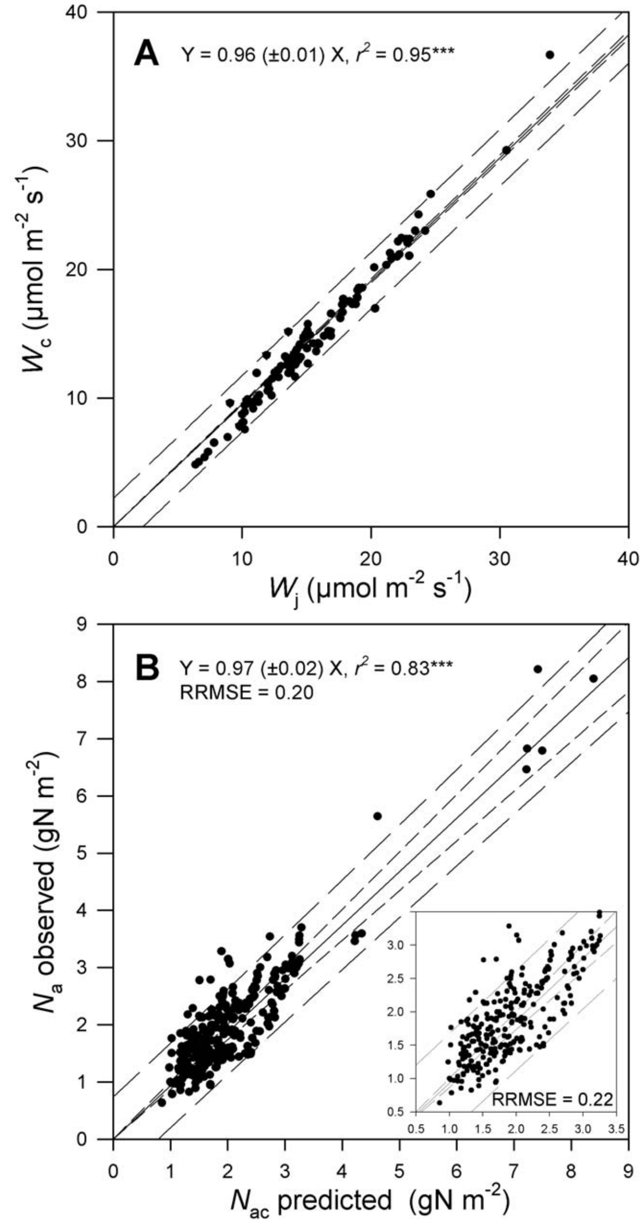

Figure 2. Tests of the coordination hypothesis using values of leaf photosynthetic traits predicted from environmental growth conditions. A) Relationship between the predicted rates of RuBP carboxylation/oxygenation (W_c) and RuBP regeneration (W_j) under plant growth conditions. B) Relationship between predicted (N_{ac}) and observed (N_a) leaf N content. The insert in Fig. 2B shows the same relationship without the very high observed N_a values for the PFT1. Symbols are as for Fig. 1.

doi:10.1371/journal.pone.0038345.g002

Prediction from Our Leaf Photosynthesis Coordination Model

Under standard environmental conditions, Np_{ac} varied significantly with k_3 and J_{fac} (Fig. 3A). Np_{ac} decreased with increasing k_3 (Fig. 3A), which imposed a strong constraint on this physiological trait. For a given leaf Np_{ac}, high values of k_3 did not affect A_n (Fig. 3B), but *PNUE* increased linearly with k_3 (Fig. 3C). For a given k_3 value, both Np_{ac} (Fig. 3A) and A_n (Fig. 3B) displayed saturating responses to increasing J_{fac}. As a consequence, *PNUE* was little affected by J_{fac} (Fig. 3C). In our model (Eqn 1), *SLA* and f_{ns} affected N_{ac}, but did not affect Np_{ac} and consequently A_n and *PNUE*. Since *SLA* displayed a higher degree of variation, the leaf structural content per unit area and consequently the leaf N content were strongly dependent on *SLA*. Thus, the leaf structural N content per unit area and the leaf N content followed an inverse relationship as *SLA* increased.

When using overall dataset means of the leaf photosynthetic traits, Np_{ac} varied significantly with radiation and temperature (Fig. 3D). Np_{ac} increased linearly with *PPFD* and decreased with Tg according to a logistic curve (Fig. 3D, Fig. S2). For a given Np_{ac}, temperature affected A_n according to a quadratic curve with an optimal Tg around 20°C although *PPFD* affected linearly A_n (Fig. 3E). As a consequence, *PNUE* was affected by Tg according to a peak curve with an optimal Tg at 25°C and was positively affected by *PPFD* according to a logarithmic curve (Fig. 3F).

Discussion

A Successful Test of the Coordination Hypothesis of Leaf Photosynthesis

The coordination hypothesis provides a testable analytical solution to predict both photosynthetic capacity and area-based leaf N content and, hence, to couple photosynthetic C gain and leaf N investment. With the large dataset used in this study, we could not falsify this testable hypothesis. Therefore, our results strongly support the validity of the leaf photosynthetic coordination hypothesis across a wide range of C_3 plant species and of environmental conditions.

Our coordination model linking leaf photosynthesis, stomata conductance and nitrogen investment has a total of 33 parameters. Only four parameters are directly related to a coordinated investment of leaf N into carboxylation capacity ($V_{C\max}$; RuBP carboxylation; Rubisco) and electron transport capacity ($J_{\max}$, RuBP regeneration; light harvesting): J_{fac}, the ratio of $J_{\max}$ to $V_{C\max}$ determines the photosynthetic capacity; and k_3, the ratio of $V_{C\max}$ to leaf photosynthetic N content (Np_{ac}) determines the fraction of metabolic leaf N invested in photosynthesis. The ratio of f_{ns} to *SLA* determines the fraction of non-metabolic N per unit total leaf N.

Photosynthetic parameter values vary to a considerable extent across species and environmental conditions in agreement with previous studies [2,3,39]. For instance, Wullschleger [2] reported that, when expressed at a reference temperature of 20°C, $V_{C\max}$ varies in the range 5–142 (µmol m^{-2} s^{-1}); $J_{\max}$ in the range 11–251 (µmol m^{-2} s^{-1}) and J_{fac} in the range 0.9–3.8 (dimensionless). Despite similar large differences in our dataset in parameter values across species and environmental conditions, our photosynthetic coordination model accounts for 93% of the total variance in N_a. Moreover, the model has a low systematic RRMSE with no systematic bias. The statistical validity of this model supports the conclusion that sunlit mature leaves of C_3 plants tend to achieve photosynthetic coordination in a wide range of both optimal and sub-optimal environmental conditions.

Along the vertical profile of C_3 plant canopies, an empirical scaling law between area based leaf N content and transmitted *PPFD* has often been reported [15,17,40,41] and has been determined as the predominant factor of N decline relative to others like leaf age or N demand [12,40,41]. Various hypotheses have been put forward to explain this observation [11,22,42,43]. Our model of the coordination hypothesis matches this scaling law, since Np_{ac} scales with radiation (*PPFD*) along the vertical canopy profile (Eqn. 2). Air temperature (T_g), relative air humidity (h_s) and ambient CO_2 concentration (C_a) also vary with depth within the canopy. At a given *PPFD*, higher h_s and lower T_g at

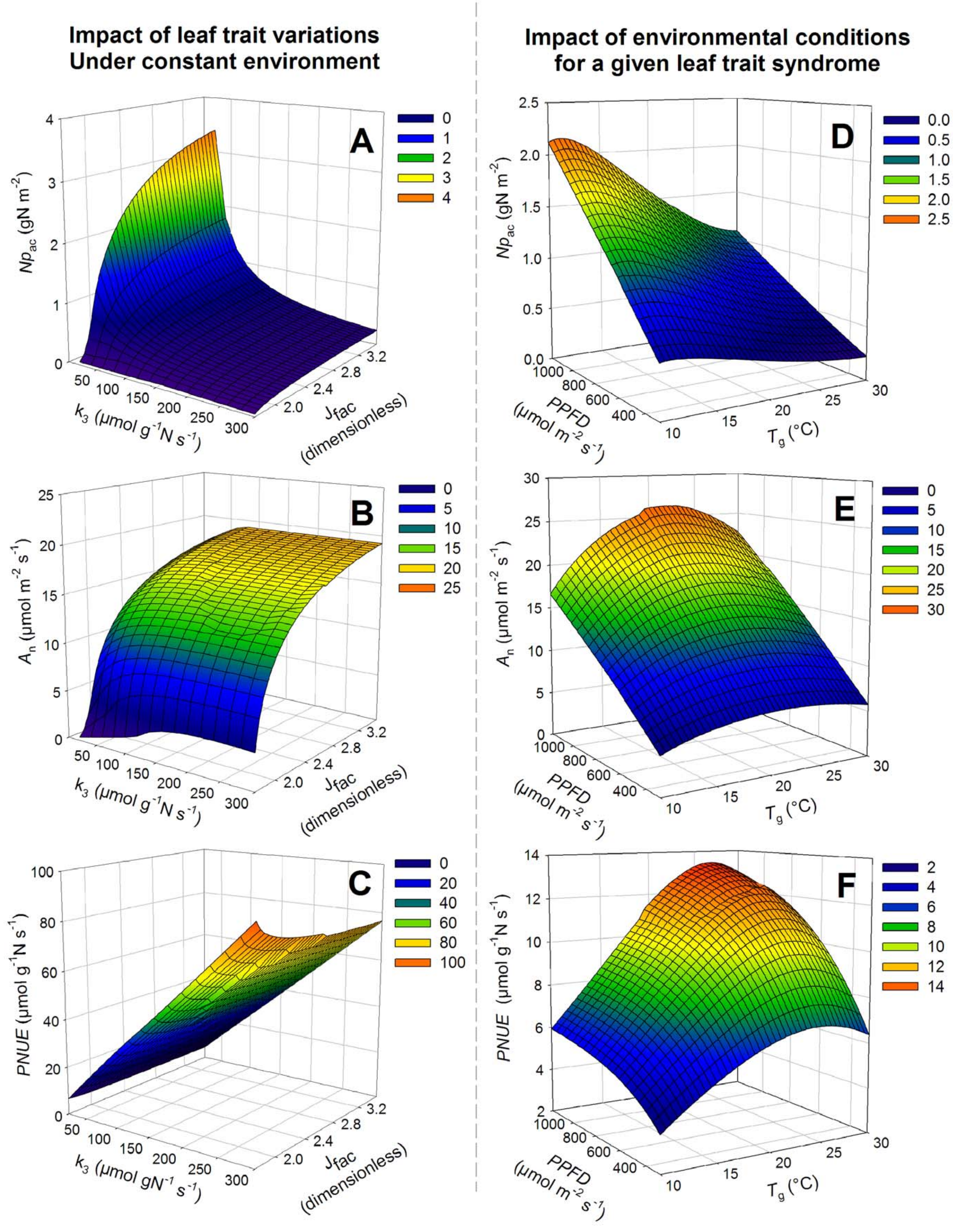

Figure 3. Relationships between simulated photosynthetic leaf N content (*Np_{ac}*) (A), net photosynthesis (*A_n*) (B) and photosynthetic N use efficiency (*PNUE*) (C) and the photosynthetic traits *k_3* and *J_{fac}* under standard mean environmental conditions (*PPFD*

= 666 µmol m^{-2} s^{-1}, T_g = 16.9°C, h_s = 0.74). k_3 is the ratio between $V_{C_{\max}}$ and Np_a. J_{fac} is the ratio between $J_{\max}$ and $V_{C_{\max}}$. A mesh of k_3 values varying between 10 and 300 µmol g^{-1} N s^{-1} with 20 steps and of J_{fac} values varying between 1.75 and 3.5 with 0.05 steps was used. Figures D–E–F, relationships between (Np_{ac}) (D), net photosynthesis (A_n) (E) and photosynthetic N use efficiency (*PNUE*) (F) and the radiation (*PPFD*) and temperature (T_g) conditions during growth. Averages over the dataset of leaf photosynthetic parameters (k_3, J_{fac} and *SLA*) are used ($k_3 = 59.1$ µmol g^{-1} N_{pa} s^{-1}, $J_{\text{fac}} = 2.45$, $SLA = 17.7$ m^2 kg^{-1} DM). The mesh for temperature is 0.5°C between 10 and 30°C and the mesh for radiation is 50 µmol m^{-2} s^{-1} between 300 and 1200 µmol m^{-2} s^{-1}. The values of h_s and T_g were fixed at 0.8 and 20°C, respectively. A_n was calculated with the coordinated leaf protein content and *PNUE* was calculated as the ratio between A_n and Np_{ac}.
doi:10.1371/journal.pone.0038345.g003

depth would reduce Np_{ac}, while a lower C_a would increase it. For some crop species like wheat, N limitation has been reported to accelerate the decline in N_a with *PPFD* [25,40,41], which may indicate preferential N allocation to leaves in full light, resulting in preferential photosynthetic coordination of these leaves despite N limitation.

Variations in photosynthetic N protein contents (Np_{ac}) appear to be an overwhelming determinant of N_a. In contrast, structural leaf N (f_{ns}) values varied only within a narrow range [38], when they were optimized by species or by PFT (from 0.0107 to 0.0135 gN g^{-1} DM for wheat and N-fixing trees, respectively, corresponding to 0.61 and 0.78 gN m^{-2} leaf when *SLA* is set to 17.6 m^2 kg^{-1} DM, dataset mean). Although optimized f_{ns} values showed little variations on a leaf dry mass basis, it accounted for 15–50% of N_a (gN m^{-2}), across all species in the dataset due to the strong variation in *SLA* across all species. Structural N is found in cell walls (1.6–9.5% of leaf N in *Polygonum cupsidatum* and 40–60% for sclerophyllous tree, shrub and vine species, [34,44]) and in nucleic acids (10–15%, [45]). In addition, other non-photosynthetic nitrogenous compounds (*e.g.* cytosolic proteins, amino acids, ribosomes and mitochondria) contribute to the structural leaf N pool [46]. Several experimental studies have attempted to estimate f_{ns}, reporting values between 0.0101 and 0.0136 gN g^{-1} DM for a range of herbaceous C_3 species [16]. These f_{ns} values are in the same range as those found for dead leaves after N resorption at senescence [47]. Structural N would therefore not be redistributed by this process [48].

Determinism of Leaf N Content Variation

Genetic and environmental factors have long been recognized to interact in determining the $A_{\max}$ vs. leaf N relationship [5]. Our study provides a means for disentangling: i) the direct environmental effects on leaf photosynthetic N content (Np_{ac}); ii) the role of photosynthetic parameters for Np_{ac} in a given environment; and iii) the response of photosynthetic parameters i.e. the plant acclimation to plant growth environment.

First, for a given set of plant parameters, positive effects of radiation and negative effects of air temperature, air relative humidity and CO_2 concentration on Np_{ac} are predicted by Eqn 2 (Fig. 3D–F). These results are in accordance with the prediction by Farquhar et al's canopy photosynthesis model [49], which links stomatal control with leaf area and leaf N content by optimizing both water and nitrogen use efficiency and predicts an increase of leaf N content and $V_{C_{\max}}$ with mean radiation increase [24,50] and mean annual rainfall [49,51]. According to the coordination hypothesis, changes in Np_{ac} affect both biochemical photosynthesis capacities, $V_{C_{\max}}$ and $J_{\max}$. Indeed, seasonal variations in $V_{C_{\max}}$ and $J_{\max}$ have been observed for a number of plant species [52,53] and were related to changes in Rubisco and cytochrome-f contents in *Polygonum cuspidatum* [54]. Including photosynthetic capacity ($V_{C_{\max}}$ and $A_{\max}$) and its relationship to leaf N content in terrestrial biosphere models resulted in substantial changes in gross primary productivity with latitude [7]. Coupled environmental variations in *PPFD*, T_K, h_s and C_a simultaneously affect Np_{ac} throughout time, which has major implications for gross primary productivity and *PNUE* of a given species or genotype.

Second, the coordination hypothesis implies that under a given environment, N_a tends toward a unique coordinated N_{ac} value (Eqn 2). As shown by the analysis of model sensitivity to parameters and input variables (Text S1, Fig. S3), k_3 and J_{fac} are among the most important determinants of N_{ac} value. Assuming a single average value of k_3 and of J_{fac} for all species in the dataset would increase N_a RRMSE by 50% (Table 3A). However, using a single J_{fac} value by PFT with species-specific k_3 and *SLA* values provided a strong accuracy for N_a prediction. This result is consistent with the strong linear relationship between $V_{C_{\max}}$ and $J_{\max}$ reported by Wullschleger [2] among 109 species, which probably indicates a phylogenetic constraint for J_{fac}. Under given environmental conditions, our results show that there is no single combination of k_3 and J_{fac} that can maximize both A_n and *PNUE* (Fig. 3A–C). Therefore, variable combinations of these photosynthetic traits could be equally relevant. This relative independency of k_3 and J_{fac} suggests that these functional traits (*sensu* [55]) correspond to possibly overlooked axes of differentiation among C_3 plant species. k_3, which modulates the N investment at a given A_n, could be related to a plant strategy of nutrients conservation [56]. J_{fac}, which increases A_n for a given k_3, could be related to a plant strategy of nutrients exploitation. However, the lack of correlation between these two photosynthetic traits and *SLA*, which is a key morphological trait separating exploitative and conservative species strategies for nutrient use [56], suggests that these physiological traits form a secondary axis of differentiation across C_3 species.

Third, some environmental growth conditions such as *PPFD*, T_g, h_s, C_a and N availability had significant effects on k_3 and J_{fac}. The increase in k_3 at low N availability tends to reduce Np_{ac} and, hence, N demand for leaf construction thereby increasing *PNUE*. The increase in k_3 with *PPFD* tends to compensate for the direct positive effect of *PPFD* on Np_{ac}, thereby lowering N demand for leaf construction under high light environments. Similarly, the decrease of k_3 with T_g mitigates the direct negative effect of temperature on Np_{ac}, thereby equalizing the N demand for a range of temperature. Mostly independently from changes in k_3 (since these two traits are not correlated across plant species), J_{fac} increases with C_a, in agreement with the lower decline under elevated CO_2 of $J_{\max}$ compared to $V_{C_{\max}}$ [33]. Moreover, J_{fac} is negatively related to *PPFD*, which is in good agreement with the higher allocation of leaf N to chlorophyll observed in low *PPFD* acclimation experiments [57]. Like the increase in k_3, the decrease in J_{fac} with *PPFD* tends to compensate for the direct positive effect of *PPFD* on Np_{ac}, especially for species with low k_3 value. Finally, the effect of temperature on J_{fac} is not significant which is in agreement with previous studies that reports constant J_{fac} with temperature (e.g. [33]).

Uncertainties in the Calculation of the Coordinated Leaf Photosynthetic N Content

Our model takes into account the two main biochemical processes controlling leaf photosynthesis as well as the biophysical process controlling stomatal conductance. Recently, leaf mesophyll conductance has also been identified as an important biophysical limitation of photosynthesis [58–60], particularly for species with low *SLA* by decreasing $V_{\mathrm{C_{max}}}$ more than $J_{\max}$ [61,62] and particularly during plant acclimation to water stress condition [58,59]. Applying mesophyll conductance in our model would first require recalculating $V_{\mathrm{C_{max}}}$ parameter from a non-rectangular hyperbola of the A_n-C_i curve and with a new set of Rubisco kinetic constants, for example [58]. Moreover, it would also require the incorporation in our model of the CO_2 diffusion mechanism between intercellular and chloroplast spaces according to a mesophyll conductance parameter [59,60]. Furthermore, the coupling between A_n and g_s leading to the calculation of A_n would require solving a new system of equations and unknowns. Finally, this would require additional mesophyll conductance data, which were not available in our dataset. The inclusion of a variable mesophyll conductance [61,62], as well as of other mechanisms implied in plant responses to water deficits [63], would allow testing the photosynthetic coordination hypothesis under severe abiotic stress conditions. With the coordination model reported here that does not include these processes, N_a values are lower than N_{ac} values under more severe abiotic stress conditions (data not shown).

The calculation of Np_{ac} relies on a number of plant parameter and environmental variables, leading to further uncertainties (see Text S1, Table S2 and Fig. S2–S3 for full details). Apart from *SLA*, k_3 and J_{fac}, all plant parameters were assumed to have a single set of values across the entire dataset (Table 2). Since the photosynthetic model was shown to be little sensitive to most of these parameters (Text S1, Fig. S3), using species-specific values would only marginally increase the accuracy of N_a prediction.

Implications

Overall, our study confirms the basic assumption of the coordination hypothesis: leaves coordinate the development of $V_{\mathrm{C_{max}}}$ and $J_{\max}$ such that W_c equals W_j. This opens opportunities to couple C and N at a global scale by incorporating the coordination hypothesis into dynamic global vegetation models (DGVMs). However, the applicability of this hypothesis for improved prediction of photosynthetic capacity and leaf nitrogen content depends on the accuracy at which we can determine key parameters of the combined photosynthesis - stomatal conductance – leaf N model as well as the timescale of plant regulatory photosynthesis mechanisms. The two key parameters J_{fac} and k_3 seem to be predictable from a combination of environmental growth conditions - probably due to the strong dependence of the development of the photosynthetic machinery on environment variables – and information about plant growth form or PFT. However, the morphological trait *SLA* does not seems to be predictable with sufficient accuracy from environmental conditions which is consistent with the large functional diversity found in a given environment [64]. *SLA* needs to be defined at least by PFT and preferably by species. This study thus confirms the relevance of leaf morphology, represented by *SLA*, in photosynthesis, which has been pointed out before, (*e.g.* [56]). However, *SLA* is one of the best-studied plant traits worldwide (*e.g.* [36]) and it may be possible to determine *SLA* with sufficient accuracy for a large range of C_3 species. Finally, although the turnover of photosynthetic enzymes like Rubisco can be seen as very constrained within the C_3 plant kingdom, to our knowledge there is no study that investigates its variability across species. We therefore stress the need for further comparative research quantifying the variability of photosynthetic enzyme turnover across C_3 species. Further tests of the coordination hypothesis will require, during plant growth, coupled measurements of microclimate, of leaf gas exchanges and of photosynthetic traits, including the dynamics of Rubisco, within the canopy [65].

Conclusion

This study bridges a gap concerning the coupling of C and N fluxes in C_3 plant species. It confirms the basic assumption of the leaf photosynthesis coordination hypothesis and demonstrates that this hypothesis can be successfully applied across species and PFTs and under a wide range of climates. Moreover, we have shown that k_3 and J_{fac} in combination with *SLA* are major plant functional traits, which reflect plant adaptation to light, temperature and N availability during growth. Surprisingly, few studies provide both leaf photosynthetic parameters and environmental conditions during plant growth. Improved datasets combining the k_3 and J_{fac} photosynthetic traits with the *SLA* morphological trait are needed to further increase our understanding of leaf economics (C–N stœchiometry) and plant strategies. The leaf photosynthesis coordination model reported here has been successfully used in a patch scale grassland vegetation model [66,67]. Further applications include modeling at regional and global scales the role of plant diversity for the carbon and nitrogen cycles.

Supporting Information

Figure S1 Details on the leaf photosynthesis coordination hypothesis. Variation of leaf carboxylation rates with leaf nitrogen content for three levels of radiations (A–C). According to the leaf photosynthesis coordination theory, a leaf photosynthetic N content is determined as colimiting the carboxylation/oxygenation of ribulose-1,5-bisphosphate (RuBP) by the enzyme ribulose 1·5-bisphosphate carboxylase/oxygenase (Rubisco; W_c), and the regeneration of RuBP by the electron transport chain (W_j). Below N_{pac}, the photosynthesis will be limited by the Rubisco activity and therefore by the amount of leaf proteins. Beyond N_{pac}, the marginal gain of photosynthesis per unit of leaf proteins is weak. Along the vertical canopy profile, N_{pac} declines with transmitted radiation when all other variables are equal.
(TIF)

Figure S2 Mean temperature functions of the maximum rates of carboxylation ($V_{\mathrm{C_{max}}}$) and electron transport ($J_{\max}$) and their ratio ($\Phi_{J_{\max}}/\Phi_{V_{\mathrm{cmax}}}$). Functions were calculated using the parameters related to temperature sensitivity (activation and deactivation enthalpies and entropy) as calibrated by Kattge & Knorr (2007) for many species (48 species for $V_{\mathrm{C_{max}}}$, 32 for $J_{\max}$ and 29 for their ratio). The error bars correspond to the standard errors among species representing the inter-specific variability.
(TIF)

Figure S3 Sensitivity analysis of the photosynthesis-stomatal conductance model. Following Félix & Xanthoulis (2005), a sensitivity analysis of the models calibrated for *Dactylis glomerata* with common one-to-one variation of parameters (±15%). Output variables are shown as lines, parameters as columns. The sensitivity index (IOS) was calculated as the maximal ratio of output variation to parameter variation during a climatic scenario (air temperature, *PPFD*, h_s and C_a) recorded from an upland site in central France (Theix, 45°43′N, 03°01′E, 870 m) for years 2003–2004. Color tones indicate sensitivity index (positive, red; negative, blue).
(TIF)

Table S1 Dataset used for the validation of leaf photosynthesis coordination. The excel file includes the leaf

photosynthetic parameters and the environmental growth conditions used to calculate W_c, W_j and N_{ac}.
(XLS)

Table S2 Range of the observed values among literature of the parameters used in the leaf photosynthesis – stomatal conductance model. The categories were the minimum, the maximum, the median and the percentage of variation of parameters range. The sources of observations were also reported. The sources, where the minimum and maximum values were observed, were annotated with – and +. A reference temperature of 20°C was used.
(DOC)

Table S3 Multiple regression analyses of Vc_{max} and J_{max} from environmental growth conditions for the bootstrap analysis. Independent variables: X_1: air CO_2 concentration (C_g); X_2: N level; X_3: soil H_2O level; X_4: radiation (*PPFD*); X_5: air growth temperature (T_g); X_6: air relative humidity (h_s). The number of observations was 236.
(DOC)

Table S4 Multiple regression analyses of k_3 and J_{fac} from environmental growth conditions for a bootstrap analysis. Independent variables were the same as Table S3. The number of observations was 236.
(DOC)

Table S5 Prediction of W_c and W_j (µmol m^{-2} s^{-1}) in using the parameters Vc_{max} and J_{max} calculated from regression analyses on the independent part of the dataset in a bootstrap analysis (Table S3). Characteristics of the W_c/W_j relationship. The intercepts of regression for each PFT were set to zero (since there were not significantly different from zero) to estimate the slopes. RRMSE: relative root mean square error.
(DOC)

Table S6 Prediction of N_{ac} in using the parameters k_3 and J_{fac} calculated from the regression analyses on the independent part of the dataset in a bootstrap analysis (Table S4). Characteristics of the relationship between predicted and observed leaf N content (N_{ac}/N_a, gN m^{-2}). The intercepts of regression for each PFT were set to zero (since there were not significantly different from zero) to estimate the slopes. Abbreviation: RRMSES and RRMSEU are systematic and unsystematic relative root mean square error, respectively.
(DOC)

Table S7 Dependence of leaf photosynthetic parameters on plant functional type (PFT). ANOVA model and mean comparison test by LSD method of the PFT effect on leaf photosynthetic traits used in the test of coordination hypothesis ($V_{C_{max}}$, J_{max}, k_3, J_{fac} and *SLA*). The values of k_3 and J_{fac} were log-transformed and all residuals followed a normal distribution. For a given variable, PFTs with the same letter belong to the same group.
(DOC)

Text S1 Sensitivity analysis of the photosynthesis – stomatal conductance model.
(DOC)

Text S2 Demonstration of the formalism of the coordinated leaf photosynthetic N content.
(DOC)

Acknowledgments

Authors thank V. Allard, N. Gross, J. Schymanski, N. Viovy and P. Ciais for constructive comments on a previous version of the manuscript.

Author Contributions

Conceived and designed the experiments: JFS VM. Analyzed the data: VM PM JK JFS. Wrote the paper: VM PM JK JFS. Assembled the data: JK VM PM FG GE. Provided model development and statistical methods: VM. Commented on the manuscript: GE SF FG.

References

1. Farquhar GD, Caemmerer Sv, Berry JA (1980) A biochemical model of photosynthetic CO_2 assimilation in leaves of C_3 species. Planta 149: 78–90.
2. Wullschleger SD (1993) Biochemical limitations to carbon assimilation in C_3 plants - A retrospective analysis of the A/C_i curves from 109 species. J Exp Bot 44: 907–920.
3. Wohlfahrt G, Bahn M, Horak I, Tappeiner U, Cernusca A (1998) A nitrogen sensitive model of leaf carbon dioxide and water vapour gas exchange: application to 13 key species from differently managed mountain grassland ecosystems. Ecol Model 113: 179–199.
4. Wohlfahrt G, Bahn M, Haubner E, Horak I, Michaeler W, et al. (1999) Inter-specific variation of the biochemical limitation to photosynthesis and related leaf traits of 30 species from mountain grassland ecosystems under different land use. Plant Cell Environ 22: 1281–1296.
5. Field CB, Mooney HA (1986) The photosynthesis-nitrogen relationship in wild plants. In: On the economy of plant form and function (ed T.J. Givnish), 25–55. Cambridge University Press, Cambridge.
6. Niinemets U, Tenhunen JD (1997) A model separating leaf structural and physiological effects on carbon gain along light gradients for the shade-tolerant species *Acer saccharum*. Plant Cell Environ 20: 845–866.
7. Kattge J, Knorr W, Raddatz T, Wirth C (2009) Quantifying photosynthetic capacity and its relationship to leaf nitrogen content for global-scale terrestrial biosphere models. Global Change Biol 15: 4 976–991.
8. Zaehle S, Sitch S, Smith B, Hatterman F (2005) Effects of parameter uncertainties on the modeling of terrestrial biosphere dynamics. Global Biogeochem Cycles 19: 1–16.
9. Haxeltine A, Prentice IC (1996) A general model for the light-use efficiency of primary production. Funct Ecol 10: 551–561.
10. Sitch S, Smith B, Prentice IC, Arneth A, Bondeau A, et al. (2003) Evaluation of ecosystem dynamics, plant geography and terrestrial carbon cycling in the LPJ dynamic global vegetation model. Global Change Biol 9: 161–185.
11. Kull O (2002) Acclimation of photosynthesis in canopies: models and limitations. Oecologia 133(3): 267–279.
12. Bertheloot J, Martre P, Andrieu B (2008) Dynamics of light and nitrogen distribution during grain filling within wheat canopy. Plant Physiol 148: 1707–1720.
13. Dreccer MF, Van Oijen M, Schapendonk A, Pot CS, Rabbinge R (2000) Dynamics of vertical leaf nitrogen distribution in a vegetative wheat canopy. Impact on canopy photosynthesis. Ann Bot 86: 821–831.
14. Dreccer MF, Slafer GA, Rabbinge R (1998) Optimization of vertical distribution of canopy nitrogen: an alternative trait to increase yield potential in winter cereals. J Crop Prod 1: 47–77.
15. Werger MJA, Hirose T (1991) Leaf nitrogen distribution and whole canopy photosynthetic carbon gain in herbaceous stands. Vegetatio 97: 11–20.
16. Schieving F, Pons TL, Werger MJA, Hirose T (1992) The vertical distribution of nitrogen and photosynthetic activity at different plant densities in *Carex acutiformis*. Plant Soil 142: 9–17.
17. Rousseaux MC, Hall AJ, Sanchez RA (1999) Light environment, nitrogen content, and carbon balance of basal leaves of sunflower canopies. Crop Sci 39: 1093–1100.
18. Johnson IR, Thornley JHM, Frantz JM, Bugbee B (2010) A model of canopy photosynthesis incorporating protein distribution through the canopy and its acclimation to light, temperature and CO_2. Ann Bot 106: 735–749.
19. Reynolds JF, Chen JL (1996) Modelling whole-plant allocation in relation to carbon and nitrogen supply: Coordination versus optimization: Opinion. Plant Soil 185: 65–74.
20. Chen JL, Reynolds JF, Harley PC, Tenhunen JD (1993) Coordination theory of leaf nitrogen distribution in a canopy. Oecologia 93: 63–69.
21. Field CB (1983) Allocating leaf nitrogen for the maximisation of carbon gain: leaf age as a control of the allocation program. Oecologia 56: 341–347.
22. Hirose T, Werger MJA (1987) Maximizing daily canopy photosynthesis with respect to the leaf nitrogen allocation pattern in the canopy. Oecologia 72: 520–526.
23. Medlyn BE (1996) The optimal allocation of nitrogen within the C_3 photosynthetic system at elevated CO_2. Aust J Plant Physiol 23: 593–603.

24. Evans JR (1989) Photosynthesis and nitrogen relationships in leaves of C_3 plants. Oecologia 78: 9–19.
25. Lötscher M, Stroh K, Schnyder H (2003) Vertical leaf nitrogen distribution in relation to nitrogen status in grassland plants. Ann Bot 92: 679–688.
26. Suzuki Y, Makino A, Mae T (2001) Changes in the turnover of Rubisco and levels of mRNAs of rbcL and rbcS in rice leaves from emergence to senescence. Plant Cell Environ 24: 1353–1360.
27. Falge E, Graber W, Siegwolf R, Tenhunen JD (1996) A model of the gas exchange response of *Picea abies* to habitat conditions. Trees-Structure Function 10: 277–287.
28. Wong SC, Cowan IR, Farquhar GD (1979) Stomatal conductance correlates with photosynthetic capacity. Nature 282: 424–426.
29. Baldocchi D (1994) An analytical solution for coupled leaf photosynthesis and stomatal conductance models. Tree Physiol 14: 1069–1079.
30. Press WH (1992) Numerical Recipes. (Cambridge University Press, New York).
31. Medlyn BE, Dreyer E, Ellsworth D, Forstreuter M, Harley PC, et al. (2002) Temperature response of parameters of a biochemically based model of photosynthesis. II. A review of experimental data. Plant Cell Environ 25: 1167–1179.
32. Kattge J, Knorr W (2007) Temperature acclimation in a biochemical model of photosynthesis: a reanalysis of data from 36 species. Plant Cell Environ 30: 1176–1190.
33. Ainsworth EA, Long SP (2005) What have we learned from 15 years of free-air CO_2 enrichment (FACE)? A meta-analytic review of the responses of photosynthesis, canopy. New Phytol 165: 351–371.
34. Onoda Y, Hikosaka K, Hirose T (2004) Allocation of nitrogen to cell walls decreases photosynthetic nitrogen-use efficiency. Funct Ecol 18: 419–425.
35. Bernacchi CJ, Pimentel C, Long SP (2003) In vivo temperature response functions of parameters required to model RuBP-limited photosynthesis. Plant Cell Environ 26(9): 1419–1430.
36. Kattge J, Díaz S, Lavorel S, Prentice IC, Leadley P, et al. (2011) TRY – a global dataset of plant traits. Global Change Biol 17: 2905–2935.
37. Willmott CJ (1982) Some comments on the evaluation of model performance. Bull Am Meteorol Soc 63: 1309–1313.
38. Maire V (2009) From functional traits of grasses to the functioning of grassland ecosystem: a mechanistic modeling approach. PhD dissertation, Blaise Pascal University, Clermont-Ferrand, France, 300p.
39. Thompson WA, Kriedemann PE, Craig IE (1992) Photosynthetic response to light and nutrients in sun-tolerant and shade-tolerant rain-forest trees.1. Growth, leaf anatomy and nutrient content. Aust J Plant Physiol 19(1): 1–18.
40. Hikosaka K, Terashima I, Katoh S (1994) Effects of leaf age, nitrogen nutrition and photon flux-density on the distribution of nitrogen among leaves of a Vine (*Ipomoea-Tricolor-Cav*) grown horizontally to avoid mutual shading of leaves. Oecologia 97(4): 451–457.
41. Hikosaka K (1996) Effects of leaf age, nitrogen nutrition and photon flux density on the organization of the photosynthetic apparatus in leaves of a vine (*Ipomoea tricolor Cav*) grown horizontally to avoid mutual shading of leaves. Planta 198(1): 144–150.
42. Schieving F, Poorter H (1999) Carbon gain in a multispecies canopy : the role of specific leaf area and photosynthetic nitrogen-use efficiency in the tragedy of the commons. New Phytol 143(1): 201–211.
43. Terashima I, Araya T, Miyazawa S, Sone K, Yano S (2005) Construction and maintenance of the optimal photosynthetic systems of the leaf, herbaceous plant and tree: an eco-developmental treatise. Ann Bot 95(3): 507–519.
44. Harrison MT, Edwards EJ, Farquhar GD, Nicotra AB, Evans JR (2009) Nitrogen in cell walls of sclerophyllous leaves accounts for little of the variation in photosynthetic nitrogen-use efficiency. Plant Cell Environ 32: 259–270.
45. Hirose T, Werger MJA, Rheenen JWAv (1989) Canopy development and leaf nitrogen distribution in a stand of *Carex acutiformis*. Ecology 70: 1610–1618.
46. Evans JR, Seemann JR (1989) The allocation of protein nitrogen in the photosynthetic apparatus: costs, consequences, and control. In: Photosynthesis (ed W.R. Briggs), 183–205. Liss, New York.
47. Hirose T, Werger MJA, Pons TL, Van Rheenen JWA (1988) Canopy structure and leaf nitrogen distribution in a stand of *Lysimachia vulgaris L.* as influenced by stand density. Oecologia 77: 145–150.
48. Lemaire G, Gastal F (1997) N uptake and distribution in plant canopies. In 'Diagnosis on the nitrogen status in crops', Ed. G. Lemaire, Springer-Verlag, Heidelberg, 3–43.
49. Farquhar GD, Buckley TN, Miller JM (2002) Optimal stomatal control in relation to leaf area and nitrogen content. Silva Fenn 36: 625–637.
50. Caemmerer Sv, Farquhar GD (1984) Effects of partial defoliation, changes of irradiance during growth, short-term water-stress and growth at enhanced $p(CO_2)$ on the photosynthetic capacity of leaves of *Phaseolus-vulgaris L.* Planta 160: 320–329.
51. Mooney HA, Ferrar PJ, Slatyer RO (1978) Photosynthetic capacity and carbon allocation patterns in diverse growth forms of Eucalyptus. Oecologia 36: 103–111.
52. Wilson KB, Baldocchi DD, Hanson PJ (2000) Spatial and seasonal variability of photosynthetic parameters and their relationship to leaf nitrogen in a deciduous forest. Tree Physiol 20: 565–578.
53. Misson L, Tu KP, Boniello RA, Goldstein AH (2006) Seasonality of photosynthetic parameters in a multi-specific and vertically complex forest ecosystem in the Sierra Nevada of California. Tree Physiol 26: 729–741.
54. Onoda Y, Hikosaka K, Hirose T (2005) Seasonal change in the balance between capacities of RuBP carboxylation and RuBP regeneration affects CO_2 response of photosynthesis in *Polygonum cuspidatum*. J Exp Bot 56: 755–763.
55. Lavorel S, McIntyre S, Landsberg J, Forbes TDA (1997) Plant functional classifications: from general groups to specific groups based on response to disturbance. Trends Ecol Evol 12: 474–478.
56. Wright IJ, Reich PB, Westoby M, Ackerly DD, Baruch Z, et al. (2004) The worldwide leaf economics spectrum. Nature 428: 821–827.
57. Evans JR, Poorter H (2001) Photosynthetic acclimation of plants to growth irradiance: the relative importance of specific leaf area and nitrogen partitioning in maximizing carbon gain. Plant Cell Environ 24: 755–767.
58. Ethier GJ, Livingston NJ (2004) On the need to incorporate sensitivity to CO_2 transfer conductance into the Farquhar-von Caemmerer-Berry leaf photosynthesis model. Plant Cell Environ 27: 137–153.
59. Flexas J, Loreto F, Niinemets U, Sharkey TD (2009) Preface: Mesophyll conductance. J Exp Bot 60: 2215–2216.
60. Niinemets U, Diaz-Espejo A, Flexas J, Galmes J, Warren CR (2009) Importance of mesophyll diffusion conductance in estimation of plant photosynthesis in the field. J Exp Bot 60: 2271–2282.
61. Pons TL, Flexas J, von Caemmerer S, Evans JR, Genty B, et al. (2009) Estimating mesophyll conductance to CO2: methodology, potential errors, and recommendations. J Exp Bot 60(8): 2217–2234.
62. Niinemets U, Diaz-Espejo A, Flexas J, Galmes J, Warren CR (2009) Role of mesophyll diffusion conductance in constraining potential photosynthetic productivity in the field. J Exp Bot 60: 2249–2270.
63. Damour G, Simonneau T, Cochard H, Urban L (2010) An overview of models of stomatal conductance at the leaf level. Plant Cell Environ 33: 1419–1438.
64. Diaz S, Hodgson JG, Thompson K, Cabido M, Cornelissen JHC, et al. (2004) The plant traits that drive ecosystems: Evidence from three continents. J Veg Sci 15: 295–304.
65. Irving LJ, Robinson D (2006) A dynamic model of Rubisco turnover in cereal leaves. New Phytol 169: 493–504.
66. Soussana JF, Maire V, Gross N, Hill D, Bachelet B, et al. (2012) GEMINI: a grassland model simulating the role of plant traits for community dynamics and ecosystem functioning. Parameterization and Evaluation. Ecol Model 231: 134–145.
67. Maire V, Soussana JF, Gross N, Bachelet B, Pagès L, et al. (2012) Plasticity of plant form and function sustains productivity and dominance along environment and competition gradients. A modeling experiment with GEMINI. Ecol Model 231 In press.